Proceedings of FEDSM'03
4TH ASME_JSME Joint Fluids Engineering Conference
Honolulu, Hawaii, USA, July 6-11, 2003

FEDSM2003-45620

FORCED CONVECTION FROM A STATIONARY CYLINDER PLACED IN A UNIFORM STREAM

László BARANYI
Dept. of Fluid and Heat Engineering, University of Miskolc
H-3515 Miskolc-Egyetemváros, Hungary

ABSTRACT

A finite difference solution is presented for 2D laminar unsteady flow around and forced convection from a stationary cylinder placed in an otherwise uniform flow. The fluid is assumed to be incompressible and of constant property. The temperature of the cylinder wall is kept constant, and the viscous energy dissipation term is neglected in the energy equation. The computed Strouhal numbers, time-mean drag and base pressure coefficients, as well as the average Nusselt numbers compare well with existing experimental results. The distribution of the local Nusselt number on the cylinder was investigated over a complete vortex shedding cycle, and shifts in *Nu* belonging to different phases were identified.
Keywords: forced convection; Navier-Stokes equations; Finite Difference Method; circular cylinder

INTRODUCTION

A huge number of researchers have investigated flow around a single circular cylinder through experimental, theoretical, and numerical approaches. Despite its simple geometry, the problem is not only extremely complex but also one with many applications. Knowledge of flow patterns around bluff bodies is important in the design of such structures as smokestacks, skyscrapers, or bridges. Long slender structures in wind often are subjected to large amplitude oscillation due to alternating vortex shedding, sometimes causing collapse of the structure. Vortex shedding can cause noisy operation of heat exchangers as the pipes of the heat exchanger vibrate.

This problem is of such practical importance that there are countless studies dealing with flow past cylinders that are fixed, oscillating, rotating, or in orbital motion. Among these, the fixed cylinder is usually the starting point of investigations, as it is relatively simple to carry out experiments on, and thus also for numerical studies, it is favored because comparison with experimental data is possible to confirm validity of the computer method used. Roshko [1], Norberg [2], and Bearman [3] are among those who have provided invaluable experimental data on flow around a fixed cylinder. Computations on the same problem have been performed by many researchers, including Kawamura and Kuwahara [4], Braza et al. [5] and Karniadakis and Triantafyllou [6].

Another aspect of importance is the heat transfer to and from fluid. Heat exchangers, hot wire anemometers, and cooling towers are some examples in which heat transfer is central; heat transfer between structures and outside air is also affected by vortex shedding.

Researchers such as Lange et al. [7] have investigated heat transfer for fixed heated cylinders in a uniform stream at low Reynolds numbers with a focus on application to hot wire anemometry. In their case, computations were also carried out at extremely low Reynolds numbers, and they claim to have identified the critical Reynolds number where vortex shedding starts as being Re=45.9.

Another low Reynolds number numerical study was carried out by Mahfouz and Badr [8] on a fixed and a rotationally oscillating cylinder for Re=40-200. They investigated the possibility of controlling heat transfer using a rotationally oscillating cylinder, and found that heat transfer was appreciably enhanced in the lock-in range, and the effect of oscillation on heat transfer was insignificant for non-lock-in cases.

The author's earlier studies dealt with computation of the flow around a fixed circular cylinder at different Reynolds numbers, from Re=10 to 1000, and up to Re=180 for an oscillating cylinder (e.g. [9]), and good agreement was obtained with experimental data for the variation of Strouhal number and time mean drag coefficient with Reynolds number. Here, further features of flow are investigated for a fixed cylinder and compared with experimental data. The base pressure coefficient, which influences the near-wake structure, is investigated and compared with the experimental data of Roshko [10]. These comparisons were used to validate the computer method used. Based on the results, the method was extended to investigate the heat transfer from a heated cylinder in which the temperature is kept constant and the fluid is assumed to be a Newtonian constant property incompressible fluid.

NOMENCLATURE

c_p : specific heat at constant pressure
C_D : drag coefficient
C_L : lift coefficient
C_{pb} : base pressure coefficient
d : cylinder diameter
D : dilation
f_v : vortex shedding frequency
h : heat transfer coefficient
J : Jacobian
k : thermal conductivity of fluid
L : length scale (=d)
Nu : Nusselt number, hd/k
p : pressure, non-dimensionalized by ρU^2
Pr : Prandtl number, $\rho\nu c_p/k$
Re : Reynolds number, Ud/ν
St : Strouhal number, $f_v d/U$
T : temperature, nondimensionalized by $\left(\tilde{T}_w - \tilde{T}_\infty\right)$
t : time, nondimensionalized by d/U
U : free stream velocity, velocity scale
u,v : velocities in x,y direction, nondimensionalized by U
x,y : Cartesian coordinates, nondimensionalized by L
ρ : fluid density

GOVERNING EQUATIONS

Constant property incompressible Newtonian fluid flow is assumed. when deriving the governing equations, which in non-dimensional forms are the Navier-Stokes equations, the equation of continuity, a Poisson equation for pressure, and the energy equation:

$$\frac{\partial u}{\partial t}+u\frac{\partial u}{\partial x}+v\frac{\partial u}{\partial y}=-\frac{\partial p}{\partial x}+\frac{1}{Re}\left(\frac{\partial^2 u}{\partial x^2}+\frac{\partial^2 u}{\partial y^2}\right); \quad (1)$$

$$\frac{\partial v}{\partial t}+u\frac{\partial v}{\partial x}+v\frac{\partial v}{\partial y}=-\frac{\partial p}{\partial y}+\frac{1}{Re}\left(\frac{\partial^2 v}{\partial x^2}+\frac{\partial^2 v}{\partial y^2}\right); \quad (2)$$

$$D=\frac{\partial u}{\partial x}+\frac{\partial v}{\partial y}; \quad (3)$$

$$\nabla^2 p=\frac{\partial^2 p}{\partial x^2}+\frac{\partial^2 p}{\partial y^2}=2\left[\frac{\partial u}{\partial x}\frac{\partial v}{\partial y}-\frac{\partial u}{\partial y}\frac{\partial v}{\partial x}\right]-\frac{\partial D}{\partial t}; \quad (4)$$

$$\frac{\partial T}{\partial t}+u\frac{\partial T}{\partial x}+v\frac{\partial T}{\partial y}=\frac{1}{Re\,Pr}\left(\frac{\partial^2 T}{\partial x^2}+\frac{\partial^2 T}{\partial y^2}\right). \quad (5)$$

The gravity force is included in the pressure terms in equations (1) and (2). At low Reynolds numbers the viscous dissipation can be neglected in the energy equation. Although the dilation D is zero by continuity (3), it is advisable to retain the term $\partial D/\partial t$ to avoid computational instability [11].

Boundary conditions:

(R_1) *cylinder surface:* $u = v = 0$;
$\frac{\partial p}{\partial n}=\frac{1}{Re}\nabla^2 v_n$;
$T_1 = 1$.

(R_2) *undisturbed domain:* $u = u_{pot}$; $v = v_{pot}$;
$\frac{\partial p}{\partial n}=\left(\frac{\partial p}{\partial n}\right)_{pot}$;
$T_2 = 0$.

Here subscript *pot* stands for potential flow, and *n* denotes the outer normal along the cylinder surface.

The heat transfer rate per unit area from the cylinder wall to the fluid can be obtained from the temperature distribution as

$$\dot{q}_w=-k_w\left(\frac{\partial \tilde{T}}{\partial \tilde{r}}\right)_w \quad (6)$$

where $\tilde{T}$ and $\tilde{r}$ are the dimensional temperature and radius, and the subscript w indicates that the temperature gradient in the radial direction is evaluated at the cylinder wall. In this study constant property fluid is considered so the thermal conductivity of the fluid k is assumed to be constant, hence $k \cong k_w$. Engineers and technicians working in this field need an expression based on measurable quantities such as

$$\dot{q}_w=h\left(\tilde{T}_w-\tilde{T}_\infty\right). \quad (7)$$

By introducing dimensionless quantities the Nusselt number Nu can be obtained as

$$Nu=\frac{hd}{k}=-\left(\frac{\partial T}{\partial R}\right)_w \quad (8)$$

where R is the dimensionless radius. The temperature gradient in the fluid should be evaluated on the cylinder surface.

TRANSFORMATION OF DOMAIN AND EQUATIONS

To avoid interpolation leading to poor solutions, a boundary-fitted coordinate system is used, allowing boundary conditions to be imposed accurately. By using unique, single-valued functions, the physical domain (x,y,t) can be mapped into a computational domain (ξ,η,τ):

$$x(\xi,\eta)=R(\eta)cos[g(\xi)];\ y(\xi,\eta)=-R(\eta)sin[g(\xi)];\ t=\tau \quad (9)$$

where the dimensionless radius

$$R(\eta)=R_1\,exp[f(\eta)]. \quad (10)$$

This choice of the structure of the mapping functions automatically assures that the obtained grid is orthogonal on the physical plane for arbitrary functions $f(\eta)$ and $g(\xi)$. In this study the following linear mapping functions are used:

$$f(\xi)=2\pi\frac{\xi}{\xi_{max}};\quad g(\eta)=\frac{\eta}{\eta_{max}}log\left(\frac{R_2}{R_1}\right) \quad (11)$$

where subscript *max* refers to maximum value. Using mapping

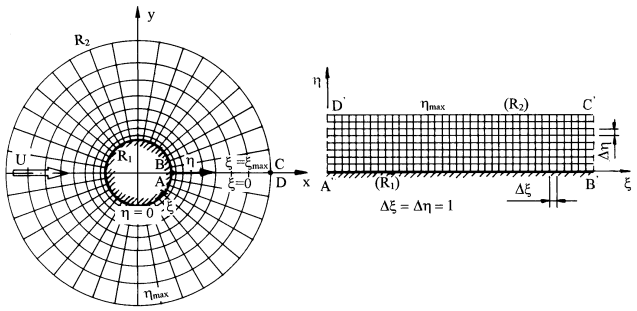

Fig. 1 Physical and computational planes

functions (11) cylindrical coordinates with logarithmically spaced radial cells are obtained on the physical plane, providing a fine grid scale near the cylinder wall and a coarse grid in the far field. Transformations (9)-(11) are single valued since in this case Jacobian J

$$J = y_\eta x_\xi - y_\xi x_\eta = \frac{2\pi \log(R_2/R_1)}{\xi_{max}\eta_{max}} R(\eta) \tag{12}$$

is positive for an arbitrary value of η in the computational domain. In equation (12) subscripts ξ and η denote differentiation. Using equations (9)-(11), the governing equations can also be transformed.

The x and y components of the transformed Navier-Stokes equations are

$$\frac{\partial u}{\partial \tau} + \frac{1}{J}\left(u\frac{\partial y}{\partial \eta} - v\frac{\partial x}{\partial \eta}\right)\frac{\partial u}{\partial \xi} + \frac{1}{J}\left(v\frac{\partial x}{\partial \xi} - u\frac{\partial y}{\partial \xi}\right)\frac{\partial u}{\partial \eta} =$$
$$-\frac{1}{J}\left(\frac{\partial y}{\partial \eta}\frac{\partial p}{\partial \xi} - \frac{\partial y}{\partial \xi}\frac{\partial p}{\partial \eta}\right) + \frac{1}{Re\,J^2}\left(g_{22}\frac{\partial^2 u}{\partial \xi^2} + g_{11}\frac{\partial^2 u}{\partial \eta^2}\right); \tag{13}$$

$$\frac{\partial v}{\partial \tau} + \frac{1}{J}\left(u\frac{\partial y}{\partial \eta} - v\frac{\partial x}{\partial \eta}\right)\frac{\partial v}{\partial \xi} + \frac{1}{J}\left(v\frac{\partial x}{\partial \xi} - u\frac{\partial y}{\partial \xi}\right)\frac{\partial v}{\partial \eta} =$$
$$-\frac{1}{J}\left(\frac{\partial x}{\partial \xi}\frac{\partial p}{\partial \eta} - \frac{\partial x}{\partial \eta}\frac{\partial p}{\partial \xi}\right) + \frac{1}{Re\,J^2}\left(g_{22}\frac{\partial^2 v}{\partial \xi^2} + g_{11}\frac{\partial^2 v}{\partial \eta^2}\right). \tag{14}$$

Dilation D transforms as

$$D = \frac{1}{J}\left(\frac{\partial y}{\partial \eta}\frac{\partial u}{\partial \xi} - \frac{\partial y}{\partial \xi}\frac{\partial u}{\partial \eta} + \frac{\partial x}{\partial \xi}\frac{\partial v}{\partial \eta} - \frac{\partial x}{\partial \eta}\frac{\partial v}{\partial \xi}\right) = 0\,. \tag{15}$$

The Poisson equation for pressure will have the form

$$g_{22}\frac{\partial^2 p}{\partial \xi^2} + g_{11}\frac{\partial^2 p}{\partial \eta^2} = 2J\left(\frac{\partial u}{\partial \xi}\frac{\partial v}{\partial \eta} - \frac{\partial u}{\partial \eta}\frac{\partial v}{\partial \xi}\right) - J^2\frac{\partial D}{\partial \tau}\,. \tag{16}$$

The energy equation transforms as

$$\frac{\partial T}{\partial \tau} + \frac{1}{J}\left(u\frac{\partial y}{\partial \eta} - v\frac{\partial x}{\partial \eta}\right)\frac{\partial T}{\partial \xi} + \frac{1}{J}\left(v\frac{\partial x}{\partial \xi} - u\frac{\partial y}{\partial \xi}\right)\frac{\partial T}{\partial \eta} =$$
$$\frac{1}{Re\,Pr\,J^2}\left(g_{22}\frac{\partial^2 T}{\partial \xi^2} + g_{11}\frac{\partial^2 T}{\partial \eta^2}\right). \tag{17}$$

Boundary conditions for pressure will be transformed as

$$R = R_1 : \frac{\partial p}{\partial \eta} = \frac{g_{11}}{Re\,J^2}\left(\frac{\partial x}{\partial \eta}\frac{\partial^2 u}{\partial \eta^2} + \frac{\partial y}{\partial \eta}\frac{\partial^2 v}{\partial \eta^2}\right); \tag{18}$$

$$R = R_2 : \quad \frac{\partial p}{\partial \eta} \cong \left(\frac{\partial p}{\partial n}\right)_{pot}. \tag{19}$$

In these equations the elements of the metric tensor will have the form

$$g_{11} = \left(\frac{\partial x}{\partial \xi}\right)^2 + \left(\frac{\partial y}{\partial \xi}\right)^2;\ g_{22} = \left(\frac{\partial x}{\partial \eta}\right)^2 + \left(\frac{\partial y}{\partial \eta}\right)^2. \tag{20}$$

The choice of transformations (9)-(11) renders the off-diagonal elements of the metric tensor zero, i.e., $g_{12} = g_{21} = 0$, and so the mixed second derivatives are missing from the Laplacian terms in equations (13), (14), (16)-(18). The transformation also ensures that the coefficients of the first order derivatives in the Laplacian terms in the above equations are zero [12]. Since the mapping is given by elementary functions, the metric parameters and coordinate derivatives can be computed from closed forms, hence numerical differentiation leading to numerical errors can be avoided.

The grid aspect ratio AR [12], i.e., the ratio of the two sides of an elementary rectangle on the physical plane (see Figure 1), will have the form

$$AR = \sqrt{\frac{g_{22}}{g_{11}}} = \frac{f_\eta}{g_\xi} = \frac{\xi_{max}\log(R_2/R_1)}{2\pi\eta_{max}}. \tag{21}$$

It can be seen from equation (21) that the grid aspect ratio is constant over the whole computational domain. By choosing the number of grid points in the ξ and η directions properly, this constant can be set to unity resulting in conformal transformation.

COMPUTATIONAL RESULTS

The author developed a computer code which is applicable to the computation of flow around a fixed or oscillating cylinder or a cylinder in orbital motion. This code calculates the velocity, pressure, and time histories of lift and drag coefficients. Several other quantities are calculated, including the vorticity distribution, stream function, the location of the front stagnation point, and the lower and upper separation points changing with time. The code has here been extended to compute the heat transfer between a heated cylinder and fluid flowing around it.

The transformed governing equations (13)-(17) are solved by the finite difference method while satisfying boundary conditions (18) and (19). The time derivatives in the transformed Navier-Stokes equations (13), (14) and in the energy equation (17) are approximated by forward differences. Fourth order central difference scheme is used for the diffusion terms and pressure derivatives. The widely used modified third order upwind scheme proposed by Kawamura and Kuwahara [4] proved to be successful in handling the convective terms in the Navier-Stokes and energy equations.

The equations of motion and equation of energy are integrated explicitly giving the velocity and temperature distributions at every time step. In the knowledge of the velocity distribution in an arbitrary time step, the pressure is calculated from equation (16) by using the successive over-

relaxation method (SOR). Dilation D is chosen to be zero at every time step. The pressure on the cylinder surface is calculated by the third order formula at every time step, shear stress on the cylinder surface is derived from the velocity distribution, and from the pressure and the shear stress we can derive the time histories of lift and drag coefficients. The non-dimensional vortex shedding frequency, Strouhal number *St* can be determined from the location of the spectrum peak of the fast Fourier transform FFT, when applied to the oscillating lift coefficient or, more cautiously, to other oscillating signals.

The dimensionless heat transfer coefficient or local Nusselt number *Nu* is obtained at every time step by using the temperature distribution

$$Nu(\varphi,t)=\frac{hd}{k}=-\left(\frac{\partial T}{\partial R}\right)_w=-\frac{1}{R_1 f'(\eta=0)}\left(\frac{\partial T}{\partial \eta}\right)_{\eta=0} \qquad (22)$$

where $f'(\eta)$ means the first derivative of f with respect to η and φ is the polar angle measured along the periphery of the cylinder. The average Nusselt number Nu is obtained as

$$Nu(t)=\frac{1}{2\pi}\int_0^{2\pi} Nu(\varphi,t)\,d\varphi\,.$$

The time averaged Nusselt number $\overline{Nu}$ can also be obtained by taking the average of $Nu(t)$ over a time period taken after reaching the quasi-steady state and covering more than one cycle.

The computational grid used is 241x131 O-mesh. The diameter of the outer boundary of computation is *30d*, where $d=2R_1$ is the cylinder diameter. Non-dimensional time steps used were usually 0.001 and 0.0005.

Momentum transfer

The author's previous studies have focused upon the computation of momentum transfer between a uniform fluid flow and a single circular cylinder, either fixed or oscillating. Good agreement was obtained for fixed cylinders against experimental results for Strouhal number and mean drag coefficient versus Reynolds number [9]. Computations for oscillating cylinders were also carried out to determine the amplitude threshold curve for locked-in vortex shedding due to crossflow cylinder oscillation [9].

The base pressure coefficient C_{pb} is a very important feature of momentum transfer. In Figure 2 time-mean values of the base pressure coefficients $\overline{C}_{pb}$ or the non-dimensional pressure measured at the farthest downstream point of the cylinder are compared with the experimental results of Roshko [10]. Agreement was good, although a discrepancy emerges at *Re*=180. This is fairly consistent with the findings of Williamson [13] that flow becomes unstable and 3-D effects begin to appear above *Re*=160. This instability was accurately predicted by the computational code. Also shown in Figure 2 are the computed root-mean-square (*rms*) values of the base pressure C_{pbrms}. Below *Re*=60, this value is very small, which is in agreement with experimental findings that vortex shedding begins between *Re*=40 and 50 [3] or, as mentioned earlier, the value of 45.9 given in [7].

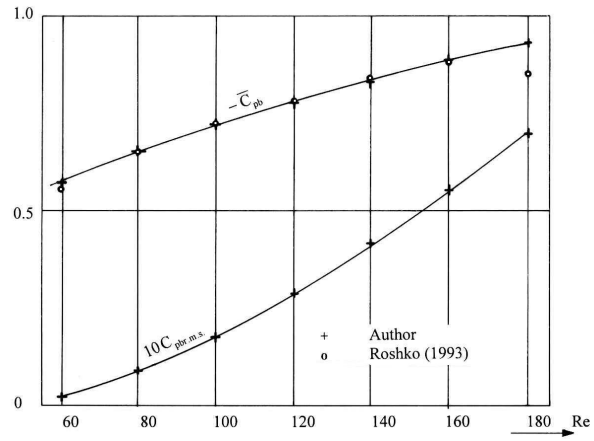

Fig. 2 Comparison of base pressures

Heat transfer

The cylinder surface is kept at constant temperature, and the temperature of the fluid flowing around it is below the cylinder temperature, meaning that heat is transferred from the cylinder surface in the fluid. To keep the cylinder surface at a constant temperature, the cylinder is heated (as is the case with hot wire anemometer). Here, it is assumed that the temperature difference is not large enough to influence the properties of the fluid (i.e. a constant property fluid).

Computations were carried out for fixed cylinders from *Re*=50 to 180, bearing in mind the experimental evidence that three-dimensional instability begins to occur at around *Re*=160, [13]. However, it should also be noted that, according to Barkley and Henderson's Floquet stability analysis, this instability starts at Re=188.5 for a cylinder of infinite aspect ratio [14]. Figure 3 shows the author's computational results for time-averaged Nusselt numbers for different Reynolds numbers up to *Re*=180, and experimentally obtained time-averaged Nusselt number $\overline{Nu}$ for heating of air flowing across a single circular cylinder, versus Reynolds number, from McAdams [15], cited in Özisik's book [16]. As can be seen, the agreement is quite good, and possibly better than it appears in the figure. This is because the solid line is only a small part of a regression curve placed on experimentally measured values over an

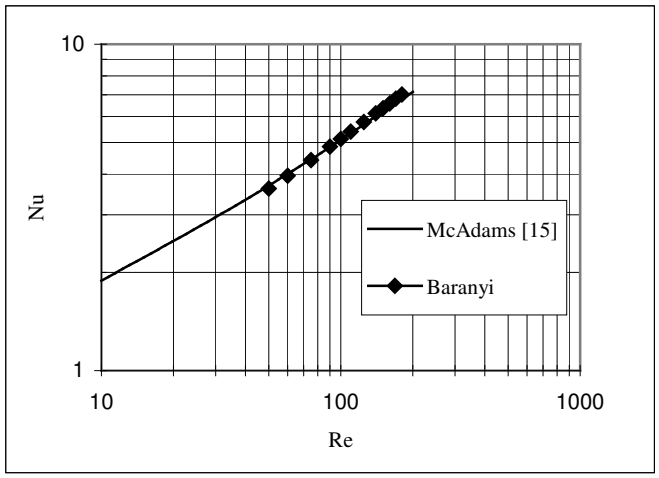

Fig. 3 Time-mean Nusselt number versus Reynolds number

extremely wide Reynolds number domain, and the real measured values in the domain under consideration here are above the regression curve itself, as are the computational results.

Table 1 summarizes computational results as a function of Reynolds number. Strouhal number, time-mean values and *rms* values of the lift and drag coefficients, base pressure coefficient, and Nusselt number are given. Note that values at higher Reynolds numbers may be influenced by three-dimensional instability. It was found that Strouhal number derived from the spectrum of the lift coefficient and that from the spectra of any other oscillating signal (C_D, C_{pb}, Nu) were somewhat different for *Re*=160 and above, and the averaged values for *St* are given in Table 1. This code shows the first appearance of three-dimensional instability from about *Re*=160.

Table 1. Time-mean and *rms* values versus *Re* number

Re	St	$\overline{C}_D$	$-\overline{C}_{pb}$	$\overline{Nu}$	C_{Lrms}	C_{Drms}	C_{pbrms}	Nu_{rms}
50	0.125	1.451	0.518	3.609	0.032	0.0001	0.0009	0.00004
60	0.137	1.419	0.574	3.950	0.093	0.0007	0.0022	0.0003
75	0.152	1.381	0.636	4.421	0.152	0.0024	0.0069	0.0008
90	0.163	1.357	0.687	4.856	0.199	0.0046	0.0129	0.0012
100	0.163	1.346	0.718	5.132	0.228	0.0064	0.0174	0.0014
110	0.171	1.338	0.747	5.396	0.256	0.0084	0.0226	0.0018
125	0.176	1.331	0.789	5.776	0.297	0.0117	0.0315	0.0027
140	0.179	1.325	0.830	6.136	0.337	0.0153	0.0413	0.0041
150	0.185	1.329	0.857	6.367	0.363	0.0178	0.0481	0.0056
160	0.188	1.330	0.883	6.590	0.388	0.0203	0.0552	0.0074
170	0.192	1.332	0.908	6.807	0.412	0.0229	0.0623	0.0094
180	0.195	1.334	0.933	7.018	0.435	0.0256	0.0696	0.0118

Figure 4 shows *rms* values of the Nusselt number versus Reynolds number. As can be seen, the amplitude of oscillation with time in the Nusselt number increases pronouncedly with increasing Reynolds number. This means that vortex shedding has an increased effect on heat transfer at larger *Re*.

The time-history of the average Nusselt number *Nu* is shown for *Re*=150 in Figure 5. In the case of a stationary cylinder, the establishment of a quasi-steady state of vortex shedding takes a relatively long time. The frequency of oscillation in the Nusselt number is the same as the frequency of oscillation for the drag coefficient, while the frequency of oscillation of the lift coefficient is half that of *Nu* and the drag coefficient. Thus, in the case of the lift coefficient, one cycle consists of two vortices shed (clockwise on the upper and counter-clockwise on the lower side), while for the drag coefficient and heat transfer, the shedding of a single vortex constitutes one cycle.

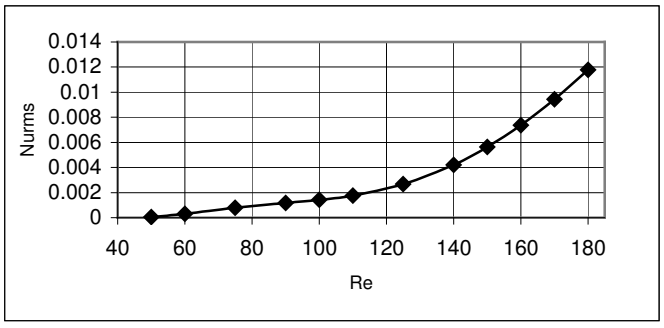

Fig. 4 *rms* value of Nusselt number versus *Re* number

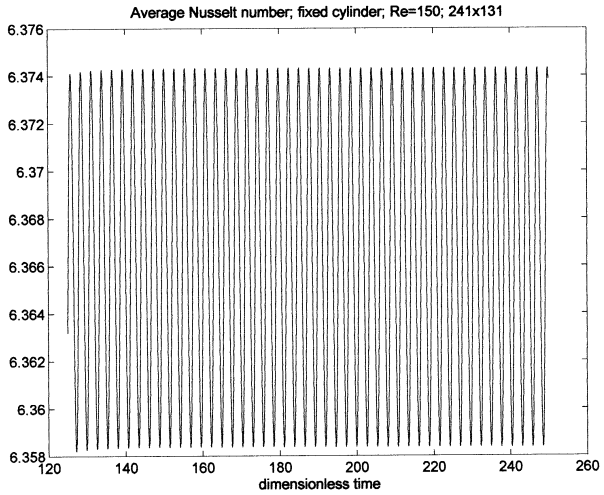

Fig. 5 Time-history of average Nusselt number

Figure 6 shows the local Nusselt number distribution for a complete cycle of vortex shedding characterized by dimensionless times t_0; $t_0 - T/4$; $t_0 - T/2$; $t_0 - 3T/4$ over the cylinder surface, for *Re*=160. Here t_0 =250 and T is the time period of a shedding cycle. As can be seen, the four curves in the figure are similar in shape and magnitude, but shift slightly over the whole periphery of the cylinder, and the shift is largest on the downstream side of the cylinder. Computations were carried out for several Reynolds numbers, and in the case of *Re*=50 it was found that the four curves for the local Nusselt number almost completely coincide, but by increasing the Reynolds number, the shift among the curves grows pronouncedly larger.

As can be seen in Figure 6, the maximum heat transfer rate is around $\varphi = 180°$, near the upstream stagnation point. This can be attributed to the thin boundary layer present at that point. As the boundary layer thickens, the local Nusselt number decreases steeply. The function seems to be completely symmetrical around this point, and minimum heat transfer

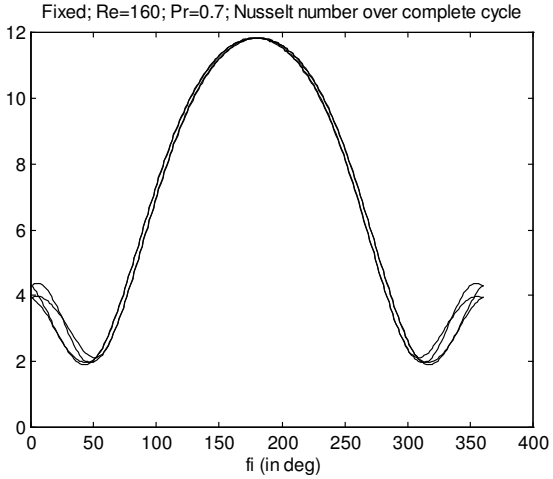

Fig. 6 Local Nusselt number on the cylinder surface

occurs not at the exactly opposite downstream point, but around 45° to each side of it. There is a local maximum in the heat

transfer at the downstream point ($\varphi = 0$) probably due to periodic vortex shedding.

The curves in Figure 6 are very similar to computational results obtained using the stream function-vorticity method [8]. These researchers showed results for *Re*=200, a somewhat unfortunate choice as they are using a two-dimensional code.

CONCLUDING REMARKS

In this study the finite difference method was applied for the numerical simulation of unsteady low-Reynolds number flow and forced convection from a stationary cylinder placed in a uniform flow. Primitive variable formulation was used for the fluid flow and the fluid was assumed to be Newtonian, incompressible and of constant property. By using boundary-fitted coordinates, interpolation of the boundary conditions becomes unnecessary. An orthogonal transformation provides a fine grid scale in the vicinity of the cylinder and a coarse grid in the far field.

Flow around a circular cylinder and forced convection from the cylinder were investigated using a code developed by the author. The non-dimensional vortex shedding frequency (Strouhal number), time-mean values of drag and base pressure coefficients, further the root-mean-square values of lift, drag, base pressure, and Nusselt number were determined for *Re*=50-180. Where possible, results were compared with experimental data and excellent agreement was obtained, except for the vicinity of *Re*=180, where three-dimensional instability might have had an influence.

The distribution of the local Nusselt number over the cylinder surface was also investigated over a complete cycle of vortex shedding. It was found that the curves belonging to different phases are similar in shape and magnitude, but shift slightly over the whole periphery of the cylinder, and the shift is largest on the downstream side of the cylinder. This shift increases with increasing Reynolds number.

The good agreement obtained between computational and experimental values encourages the author to extend the investigation in the future to the case of forced convection from an oscillating cylinder, and to develop a three-dimensional code.

ACKNOWLEDGMENTS

The support provided by the Hungarian National Research Foundation (project No. T030024) is gratefully acknowledged.

REFERENCES

[1] Roshko, A., 1954, "On the development of turbulent wakes from vortex streets," NACA Rep. 1191.

[2] Norberg, C., 2001, "Flow around a circular cylinder: aspects of fluctuating lift," *Journal of Fluids and Structures*, **15**, pp. 459-469.

[3] Bearman, P.W., 1997, "Developments in the understanding of bluff body flows," *Proc. JSME Centennial Grand Congress, International Conference on Fluid Engineering*, **1**, Tokyo, pp. 53-61.

[4] Kawamura, T. and Kuwahara, K., 1984, "Computation of high Reynolds number flow around a circular cylinder with surface roughness,'' *Proc. of the 22nd Aerospace Sciences Meeting*, Reno, Nevada, AIAA-84-0340, pp. 1-11.

[5] Braza, M., Chassaing, P. and Minh, H. H., 1986, "Numerical study and physical analysis of the pressure and velocity fields in the near wake of a circular cylinder," *Journal of Fluid Mechanics*, **165**, pp. 79-130.

[6] Karniadakis, G.E. and Triantafyllou, D.S., 1989, "Frequency selection and asymptotic states in laminar wakes," *Journal of Fluid Mechanics*, **199**, pp. 441-469.

[7] Lange, C.F., Durst, F. and Breuer, M., 1998, "Momentum and heat transfer from cylinders in laminar crossflow at $10^{-4} \le Re \le 200$," *International Journal of Heat and Mass Transfer*, **41**, pp. 3409-3430.

[8] Mahfouz, F.M. and Badr, H.M., 2000, "Forced convection from a rotationally oscillating cylinder placed in a uniform stream," *International Journal of Heat and Mass Transfer*, **43**, pp. 3093-3104.

[9] Baranyi, L. and Shirakashi, M., 1999, "Numerical solution for laminar unsteady flow about fixed and oscillating cylinders," *Computer Assisted Mechanics and Engineering Sciences*, **6**, pp. 263-277.

[10] Roshko, A., 1993, "Perspectives on Bluff Body Aerodynamics," *Journal of Wind Engineering and Industrial Aerodynamics*, **49**, pp. 79.

[11] Harlow, F.H. and Welch, J.E., 1965, "Numerical calculation of time-dependent viscous incompressible flow of fluid with free surface," *Physics of Fluids*, **8**, pp. 2182-2189.

[12] Fletcher, C.A.J., 1997, *Computational Techniques for Fluid Dynamics*, Vol. 2, Springer, 2nd edition, Berlin.

[13] Williamson, C.H.K., 1996, "Vortex dynamics in the cylinder wake," *Annual Review of Fluid Mechanics*, **28**, pp. 477-539.

[14] Barkley, D. and Henderson, R.D., 1996, "Three-dimensional Floquet stability analysis of the wake of a circular cylinder," *Journal of Fluid Mechanics*, **322**, pp. 215-241.

[15] McAdams, W.H., 1954, *Heat Transmission*, McGraw-Hill, 3rd edition, New York.

[16] Özisik, M.N., 1985, *Heat Transfer*, *A Basic Approach,* McGraw-Hill, New York.